Depth-profiling X-ray photoelectron spectroscopy (XPS) analysis of interlayer diffusion in polyelectrolyte multilayers

Citation: Gilbert, J. B. et al. "Depth-Profiling X-Ray Photoelectron Spectroscopy (XPS) Analysis of Interlayer Diffusion in Polyelectrolyte Multilayers." Proceedings of the National Academy of Sciences 110, 17 (April 2013): 6651–6656 © 2013 The Authors

As Published: http://dx.doi.org/10.1073/PNAS.1222325110

Publisher: National Academy of Sciences (U.S.)

Persistent URL: http://hdl.handle.net/1721.1/116225

Version: Final published version: final published article, as it appeared in a journal, conference proceedings, or other formally published context

Depth-profiling X-ray photoelectron spectroscopy (XPS) analysis of interlayer diffusion in polyelectrolyte multilayers

Jonathan B. Gilbert[a], Michael F. Rubner[b,1], and Robert E. Cohen[a,1]

Departments of [a]Chemical Engineering and [b]Materials Science and Engineering, Massachusetts Institute of Technology, Cambridge, MA 02139

Edited by Michael L. Klein, Temple University, Philadelphia, PA, and approved March 12, 2013 (received for review December 20, 2012)

Functional organic thin films often demand precise control over the nanometer-level structure. Interlayer diffusion of materials may destroy this precise structure; therefore, a better understanding of when interlayer diffusion occurs and how to control it is needed. X-ray photoelectron spectroscopy paired with C_{60}^+ cluster ion sputtering enables high-resolution analysis of the atomic composition and chemical state of organic thin films with depth. Using this technique, we explore issues common to the polyelectrolyte multilayer field, such as the competition between hydrogen bonding and electrostatic interactions in multilayers, blocking interlayer diffusion of polymers, the exchange of film components with a surrounding solution, and the extent and kinetics of interlayer diffusion. The diffusion coefficient of chitosan (M = ~100 kDa) in swollen hydrogen-bonded poly(ethylene oxide)/poly(acrylic acid) multilayer films was examined and determined to be $1.4*10^{-12}$ cm^2/s. Using the high-resolution data, we show that upon chitosan diffusion into the hydrogen-bonded region, poly(ethylene oxide) is displaced from the film. Under the conditions tested, a single layer of poly(allylamine hydrochloride) completely stops chitosan diffusion. We expect our results to enhance the understanding of how to control polyelectrolyte multilayer structure, what chemical compositional changes occur with diffusion, and under what conditions polymers in the film exchange with the solution.

XPS depth profiling | layer-by-layer films | interdiffusion

Layer-by-layer assembly of polyelectrolyte multilayers (PEMs) allows for the precise deposition of ultrathin organic films that can conformally coat features of any shape and size. These films can incorporate a variety of species, leading to a wide range of applications, including antifogging (1), antireflection (2), drug delivery (3–7), fuel cells (8), and responsive materials (9). Because the multilayer films are assembled through a sequential self-limiting adsorption process onto a substrate (10), a major advantage of the technique is the ability to constrain the location of certain materials within the film at the nanoscale simply by controlling the order of material deposition. Such nanoscale spatial control has allowed the creation of complex periodic heterostructures not easily realized by other deposition techniques (11). In some cases, however, diffusion of the constituent macromolecular species in and out of the film may occur, changing the desired film stratification, composition, growth profile, and properties (12). This type of diffusion, known as interlayer diffusion, often is detrimental to the desired properties but also might be an opportunity to impart new functions. However, interlayer diffusion has proven difficult to fully characterize and control and a more thorough understanding is needed.

Interlayer diffusion in PEM films may be detrimental if the desired stratified heterostructure is lost during the assembly process, during a postassembly treatment, or in use. For example, in the cases of the sequential release of therapeutics (7), structural color (13), organic light-emitting diode devices (14), solar cells (15), and on-demand release of PEM films (5, 16), the loss of stratification due to interlayer diffusion results in loss of the desired function. However, in other cases, such as surface planarization for the creation of higher-efficiency dye-sensitized solar cells (15) or ordering of the internal or surface arrangement of PEM films (17, 18), interlayer diffusion may be harnessed to provide functional benefits. Interlayer diffusion also may be used to tune material properties such as the critical dissolution pH in hydrogen-bonding systems through the addition of small amounts of electrostatic cross-links (16) or viscoelasticity through diffusion of stiffer polymer components (19). In all these cases, interlayer diffusion must be understood and controlled.

Interlayer diffusion also affects the mechanism of PEM film growth. Some polymer systems show linear growth where the bilayer thickness is invariant with deposition cycles, whereas other systems show exponential growth with progressively increasing bilayer thicknesses (20). It is widely believed that exponential growth arises from rapid interlayer diffusion of polymers throughout the film during the fabrication steps (20, 21); however, some disagree with this conclusion (22). Improved analytic techniques that provide spatial information about the location of specific molecules within a multilayer thin film therefore clearly are needed.

Because of the importance of understanding interlayer diffusion, a variety of techniques have been used to analyze it, with varying degrees of success. These techniques include confocal microscopy (23–25), FRET (26, 27), FTIR (28), neutron reflectivity (29–31), and X-ray reflectometry (32). Confocal microscopy is limited in spatial sensitivity, as films much thicker than the typical PEM thickness (≤500 nm) are required because of a relatively low z-resolution (23–25). FRET is more sensitive but relies on fluorescent modification of polymers for indirect measurements of diffusion (26, 27). FTIR may provide valuable information on the exchange of polymers in solution with PEM film components but commonly probes the full thickness of the film, limiting the ability to spatially resolve the effects of diffusion (28). Neutron reflectivity and X-ray reflectometry (29–32) require nuclear contrast and electron density contrast, respectively, in the film and commonly require the use of special deuterated polymers. In comparison, X-ray photoelectron spectroscopy (XPS) is a highly sensitive surface analysis method that probes the top 10 nm of a film. When combined with sputtering or etching sources to remove material slowly between analysis cycles without damaging underlying material, depth-profiling XPS enables high-resolution chemical analysis of polymer films. The information provided by this technique might expand the understanding of how to control PEM structure, what compositional/structural changes occur with interlayer diffusion, and when polymers in the film exchange with deposition/postassembly solutions.

Development of less destructive sputtering or etching sources has been the enabling step in advancing polymer depth-profiling capabilities. Many depth-profiling techniques use single-atom sputtering sources such as argon, applicable to inorganic materials but severely damaging to polymers (33–35). Only recently have cluster ion sources such as C_{60}^+ been used in conjunction with XPS for analysis of polymer films with depth (33, 36, 37). Cluster ion C_{60}^+ sputtering

Author contributions: J.B.G., M.F.R., and R.E.C. designed research; J.B.G. performed research; J.B.G., M.F.R., and R.E.C. analyzed data; and J.B.G., M.F.R., and R.E.C. wrote the paper.

The authors declare no conflict of interest.

This article is a PNAS Direct Submission.

[1]To whom correspondence may be addressed. E-mail: recohen@mit.edu or rubner@mit.edu.

This article contains supporting information online at www.pnas.org/lookup/suppl/doi:10.1073/pnas.1222325110/-/DCSupplemental.

is much less damaging because the energy transfer from the ion to the material occurs primarily at the surface, minimizing the chemical damage deep into the film (38). Therefore, most of the damaged material is removed from the surface, minimizing its interference with the proper analysis of the exposed surface (39).

One strategy in the fabrication of functional PEM films is the use of blocking layers to minimize interlayer diffusion. Earlier studies (7, 24, 40–42) showed that the properties of a successful blocking layer depend on the diffusing species under consideration and the conditions of diffusion. Some have found that covalent cross-linking is the only way to stop interlayer diffusion of polymers (7, 43), whereas others have noted that electrostatic interactions may be used to stop interlayer diffusion (24, 44, 45). Of interest to this study is how blocking layers enable the controlled production of free-floating PEM films by maintaining the desired dissolution properties of a sacrificial region that anchors a pH-stable PEM film to a substrate surface. Once released, these free-floating assemblies have been used for tissue engineering (46) and drug delivery (5, 6).

In this paper, we designed a model system that enables the study of common attributes of interlayer diffusion found in many PEM systems, including blocking-layer effectiveness. The sacrificial component of this model PEM system is a hydrogen-bonded region [poly(acrylic acid)/poly(ethylene oxide)] (PAA/PEO) that is insoluble at low pH but becomes soluble at a critical higher pH. A pH-stable PEM system based on chitosan and hyaluronic acid (HA) is assembled on top of this sacrificial region with the goal of creating an on-demand pH-triggered release of the chitosan /HA multilayer films. Previously, we used a related approach to create cellular backpacks that attach to immune system cells via specific interactions between HA and CD-44 receptors on the cell surface (5). From these earlier studies, it became apparent that the assembly of chitosan /HA onto a hydrogen-bonded region rendered the entire multilayer system insoluble under pH conditions that should dissolve the sacrificial region. Thus, this work seeks to determine whether interlayer diffusion of chitosan/HA causes the changes in solubility and how suitable blocking layers can prevent these changes. From a fundamental perspective, this model system allows the exploration of elements such as the competition between hydrogen bonding and electrostatic interactions in multilayers, the design of an effective blocking layer, the exchange of film components with a surrounding solution, and the extent and kinetics of interlayer diffusion. Using XPS depth-profiling data acquired with C_{60}^+ cluster ion sputtering, we find that chitosan diffuses effectively into the hydrogen-bonded region of the multilayer film and displaces the hydrogen-bonded component PEO. In addition, we show that this interlayer diffusion process may be blocked completely with only a single adsorbed layer of a polycation.

Results and Discussion

The model PEM films examined in this work were assembled on glass slides coated with an 80-nm poly(diallyldimethylammonium chloride) (PDAC) and poly(styrene sulfonate) (SPS) adhesion-promoting multilayer. Above this adhesion layer, was a hydrogen-bonded film composed of PAA and PEO. The solubility of this hydrogen-bonded PEM system is pH sensitive, and above a pH of 3.6, it will dissolve in water (47). Fig. 1 shows a cartoon representation of the multilayer heterostructures examined in this work, along with the experimentally determined thicknesses of the various regions of the multilayer. In Fig. 1*A*, the experiments involved immersing a hydrogen-bonded multilayer film in a chitosan solution for varying amounts of time. In Fig. 1*B*, blocking layers containing varying numbers of poly(allylamine hydrochloride) (PAH) and SPS layers were deposited on top of the hydrogen-bonded region followed by the assembly of a multilayer of HA and chitosan.

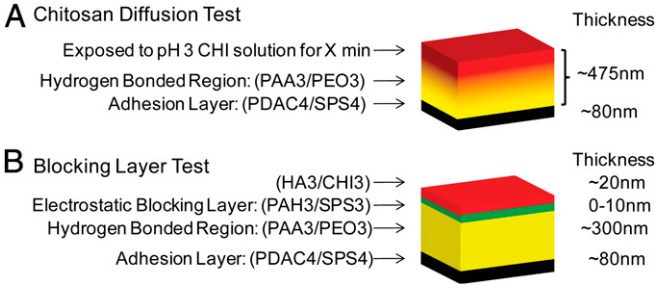

Fig. 1. Schematic of systems used to test (*A*) chitosan (CHI) diffusion into the hydrogen-bonded region and (*B*) electrostatic blocking-layer effectiveness. The number after the polymer abbreviation is the deposition solution pH.

These stratified films were dried then analyzed using depth-profiling XPS paired with C_{60}^+ sputtering to collect C1s, O1s, N1s, and Si2p high-resolution spectra. It is important to note that prolonged X-ray exposure and C_{60}^+ sputtering may alter the chemical composition of PEMs and decrease the interface resolution (36, 48). As described in Fig. S1, the choice of XPS data acquisition parameters and sputtering conditions is very important because long periods of X-ray exposure reduced the O-to-C ratio, particularly the signal of the carboxyl peak at ~289 eV (49). As a result, we chose acquisition parameters and C_{60}^+ sputtering conditions to minimize the total X-ray exposure time while still obtaining an acceptable resolution and signal-to-noise ratio at each point in the depth profile.

Diffusion of Chitosan in Hydrogen-Bonded Multilayers. To explore the question of whether the adsorbed chitosan diffuses into the swollen hydrogen-bonded region and by how much, the nitrogen signal from the amine on chitosan was analyzed as a function of depth for hydrogen-bonded multilayers exposed to a 0.1% (wt/vol) CHI solution at pH 3 for a specified amount of time. The chitosan solution acted as an infinite supply for diffusion of chitosan into the hydrogen-bonded region. All samples were rinsed with water for 4 min and dried with nitrogen gas before analysis. The compiled spectra for chitosan exposure times of 1, 3, 10, and 60 min (CHI1, CHI3, CHI10, and CHI60) are plotted in Fig. 2 *A–D*. Color was added to highlight the approximate locations of the distinct regions of the PEM film, using the same color scheme shown in Fig. 1*A*. The depth of the (red) chitosan region was determined by analyzing the intensity of the N1s signal with depth. When the N1s signal dropped to background levels, the spectrum was colored yellow to denote the hydrogen-bonded region. Finally, the (black) adhesion layer starts when the N1s signal increases at the base of the film as a result of the presence of nitrogen-containing PDAC.

The spectra from Fig. 2 *A–D* were analyzed to determine the atomic percentage of nitrogen with depth, as seen in Fig. 2*E*. A film not exposed to chitosan is shown in Fig. S2. The concentration of nitrogen in the multilayer film increased systematically with time of exposure to the chitosan solution. Also, the maximum depth at which an appreciable nitrogen signal was observed increased with time. Separate experiments showed that the PDAC from the adhesion layers does not enter the hydrogen-bonded region during the assembly process, even after many hours at pH 3 (Fig. S2). Thus, the only source of nitrogen in the film, above the 80-nm adhesion layer, is from the chitosan that diffused from the top of the hydrogen-bonded region. For the samples CHI1, CHI3, and CHI10, the location of the diffusion front (where N1s concentration is 50% of the maximum value) advanced 181, 238, and 299 nm, respectively, as measured in dry films. Because the final dry thickness remained relatively constant, independent of chitosan diffusion depth, the diffusion of chitosan does not expand or collapse the film greatly. As a result, the dry diffusion distance of chitosan directly correlates with the thickness of the portion of the (PAA3/PEO3) film that was altered by chitosan diffusion. Therefore, to estimate the diffusion coefficient, the chitosan penetration distances were multiplied by a factor of 2.5 to account for the 250% swelling of the (PAA3/PEO3) film in pH 3 water (Table 1 and Table S1). After 60 min in the chitosan solution (CHI60), the chitosan diffused through the entire hydrogen-bonded region, as seen by the uniformly high nitrogen content throughout the film in Fig. 2*E*. These results clearly show that the adsorbed chitosan diffuses into the hydrogen-bonded region. Chitosan is known to be highly diffusive because of a charge density lower than that of typical polyamines, such as PAH, and the presence of multiple hydrogen-bonding acceptors (25, 26).

To estimate the diffusion coefficient of chitosan into the hydrogen-bonded region, we used the data in Table 1 and the

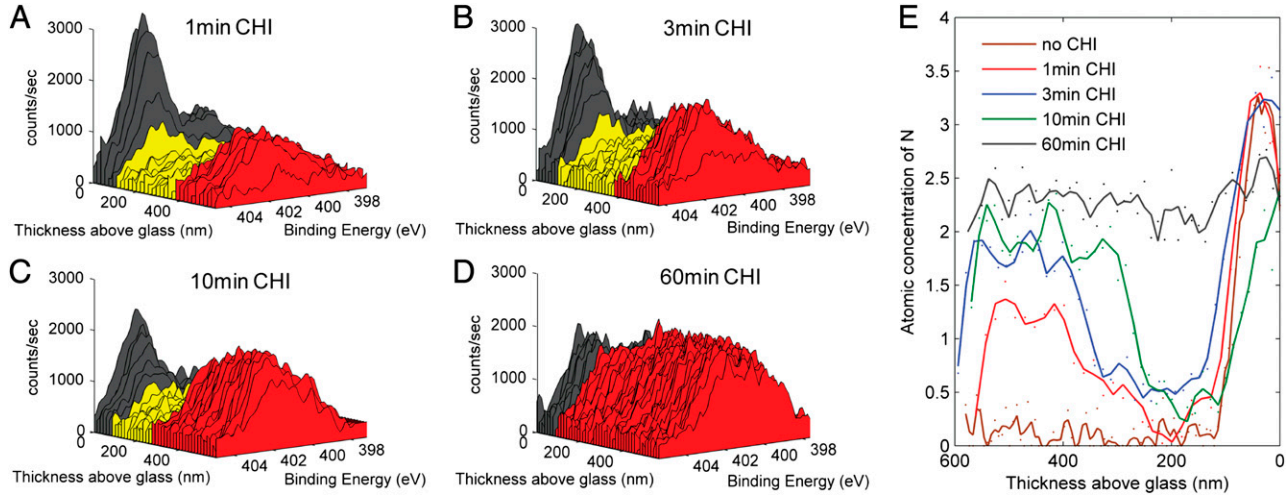

Fig. 2. Diffusion of chitosan into hydrogen-bonded films. Spectra of hydrogen-bonded (PAA3/PEO3) films exposed to chitosan solution for different amounts of time: (*A*) 1-min exposure, (*B*) 3-min exposure, (*C*) 10-min exposure, and (*D*) 60-min exposure to chitosan. The color scheme is the same as that of Fig. 1*A*. Red spectra represent chitosan-infused areas, yellow spectra represent the hydrogen-bonded (PAA3/PEO3) area, and black spectra represent the (PDAC4/SPS4) adhesion layer. (*E*) Quantification of *A*–*D* to determine the atomic concentration of nitrogen with depth in the film. Data points are individual dots, and the lines show the result of a Savitzky–Golay five-point quadratic algorithm.

characteristic diffusion length, $L = \sqrt{4Dt}$ (50). As seen in Table 1, the calculated diffusion coefficient is consistent for the three time points sampled and is ~$1.4*10^{-12}$ cm^2/s. Recent reports on interlayer diffusion coefficients in polyelectrolyte multilayers range from 10^{-20} cm^2/s for SPS in linearly growing (PAH/SPS) films (29) to 10^{-7} cm^2/s for poly(L-lysine) in exponentially growing poly(L-lysine)/HA films (20). This wide range of reported interlayer diffusion coefficients is the result of a fundamental difference in the film growth mechanism between linearly and exponentially growing films. In linear growth conditions, the deposited polymers generally interact only with the top surface and thus generally have interlayer diffusion coefficients below 10^{-17} cm^2/s (29–31). In comparison, exponentially growing systems require some amount of interlayer diffusion to occur during the dipping cycle (20) and, as a result, have higher reported interlayer diffusion coefficients, in the range of 10^{-16} to 10^{-7} cm^2/s depending on the conditions and polyelectrolytes used (20, 26). A recent paper by Lundin et al. (26) used FRET and showed that the interlayer diffusion of chitosan in exponentially growing films made of chitosan and heparin was ~10^{-15} cm^2/s for 150-kDa chitosan. Our reported interlayer diffusion coefficient of ~10^{-12} cm^2/s for chitosan of roughly the same molecular weight is larger but well within the range of other exponentially growing polymer systems previously studied. In addition, the diffusion coefficient we report would be higher than the diffusion coefficient of chitosan in a pure film of chitosan/heparin, as Xu et al. (30) showed that weaker matrix interactions enable a higher diffusion coefficient. Given that in our study chitosan diffused in a hydrogen-bonded (PAA3/PEO3) matrix with a low interaction strength, as measured by dissolution pH, and did not have an internal structure, as measured by neutron reflectivity (51), it thus would allow for a diffusion coefficient higher than that of the more strongly interacting electrostatic matrix of chitosan and heparin.

Table 1. Diffusion of chitosan in a swollen hydrogen-bonded film

Sample	*t*, s	Dry film distance, nm	Swollen film distance, nm	D, cm^2/s
CHI1	360	181	452	1.42E-12
CHI3	720	238	594	1.23E-12
CHI10	900	299	748	1.56E-12

Dry distance multiplied by 2.5 to account for 250% film swelling at pH 3. D, distance; *t*, time.

Displacement of PEO from Film by Chitosan. One possible effect of interlayer diffusion in PEMs is the displacement of materials from the film into solution (28, 40, 52). In our model system, interlayer diffusion of chitosan into the hydrogen-bonded region changes the dominant interaction from hydrogen bonding between PAA and PEO to electrostatic interactions between PAA and chitosan. FTIR confirmed these new electrostatic interactions. In films with large amounts of chitosan diffusion, the PAA ionization level increased as a result of the titration of carboxylic acid groups to carboxylate groups by cationic chitosan (Fig. S3) (53). Therefore, upon chitosan diffusion, electrostatic interactions between chitosan and PAA displace the weaker hydrogen-bonding interactions between PEO and PAA. As a result, the hydrogen-bonding acceptor PEO no longer is associated with the film and may diffuse out.

Enabled by the high sensitivity of XPS, PEO displacement can be explored directly. Fig. 3 shows the high-resolution C1s data from the CHI1 and CHI3 samples using the color scheme from Fig. 1*A* (CHI10 and CHI60 data in Fig. S4). The red region is infiltrated with chitosan, and its location in this region was determined by analyzing the intensity of the N1s signal with depth as in Fig. 2. In the remaining depth of the film, the N1s signal is very low (<0.5% atomic conc. N), signifying that in this yellow region, the film contains little to no chitosan. To analyze the displacement of PEO from the film, the C1s spectra from the (red) chitosan-infiltrated regions were compared with the spectra in the (yellow) hydrogen-bonded regions of the film. In particular, we focused on the change in C1s signal intensity at 286.5 eV. Both PEO and chitosan have a signal at this point, but because the extent of chitosan diffusion can be determined independently by the nitrogen signal, the changes in C1s spectra may be used to analyze the displacement of PEO from the film. The C1s spectra of pure PEO, chitosan, and PAA may be seen in Fig. S5.

As shown in Fig. 3 *A* and *B*, the red regions, where chitosan has diffused into the film, have a markedly lower signal at 286.5 eV than the yellow hydrogen-bonded region. The change in signal intensity at 286.5 eV is highlighted in Fig. 3*C*, which compares the chitosan-infiltrated regions from Fig. 3 *A* and *B* with the (PAA3/PEO3) hydrogen-bonded region. The spectra of all chitosan-exposed samples were obtained from ~450 nm above the glass surface to minimize differences due to X-ray exposure time or C_{60}^+ sputtering time. The decrease in signal intensity at 286.5 eV is a result of chitosan diffusion displacing PEO and

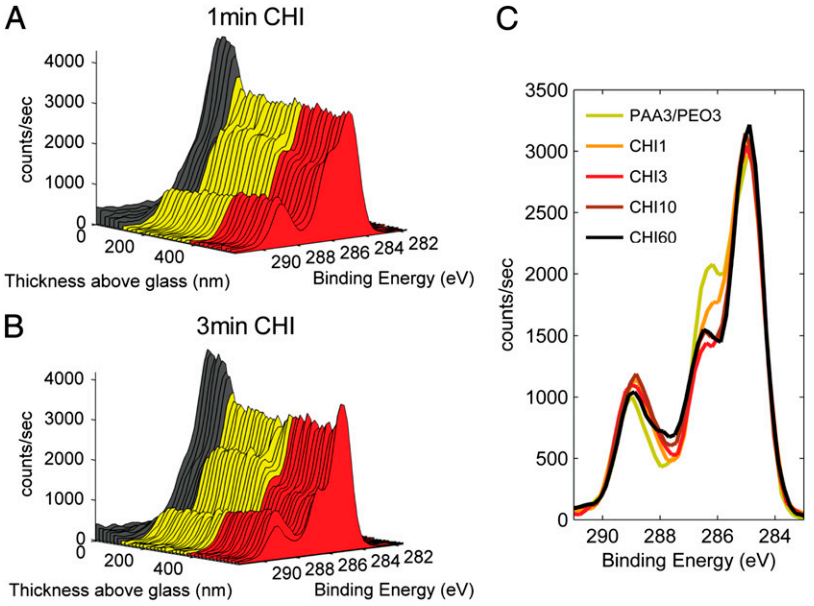

Fig. 3. High-resolution C1s XPS depth profiling of a hydrogen-bonded film exposed to chitosan solution for (*A*) 1 min and (*B*) 3 min. The color scheme is the same as that of Fig. 1*A*. Red spectra represent chitosan-infused areas, yellow spectra represent the hydrogen-bonded (PAA3/PEO3) areas, and black spectra represent the (PDAC4/SPS4) adhesion layer. Comparing the red chitosan-diffused areas with the yellow hydrogen-bonded areas, the chitosan-diffused areas have a lower signal at 286.5 eV because PEO has diffused out. (*C*) Comparison of C1s spectra with different chitosan-exposure times with the initial yellow hydrogen-bonded area. The longer the exposure to chitosan solution, the more the PEO signal at 286.5 eV decreases. All chitosan-exposed spectra were from ~450 nm above the glass surface.

allowing it to diffuse out of the film. Because chitosan also has a peak at 286.5 eV, if PEO was not diffusing out of the film, this signal would increase. Fig. 3*C* also shows that the decrease in the signal at 286.5 eV correlates with the holding time in chitosan solution, which is consistent with the diffusion of PEO out of the film.

Electrostatic Blocking Layer Stops Chitosan Diffusion. In many cases, it is desirable to stop interlayer diffusion to maintain distinct functional regions of a multilayer heterostructure. The effect of electrostatic blocking layers on the diffusion of chitosan into the hydrogen-bonded region was investigated using the film architecture shown in Fig. 1*B*. Unlike the previous study, above the hydrogen-bonded region there is an electrostatic blocking layer that varies from a single layer of PAH (<1 nm) to 9.5 bilayers of PAH3/SPS3 (10 nm). On top of the blocking region, the final region is a 20-nm HA3/CHI3 multilayer film. To determine the location of the distinct regions of the PEM film and apply the color scheme shown in Fig. 1*B*, information from the C1s and N1s spectra was combined. For example, in Fig. 4*A*, the transition from the red HA/CHI region at the surface to the green (PAH3/SPS3) blocking region was determined by the change in shape of the C1s spectrum. The shape change is a result of more carbon–carbon bonds at 285 eV and fewer carbon–oxygen bonds at 286.5 eV in the green region compared with the red region. Because XPS analyzes approximately the top 10 nm and the blocking layers are less than 10 nm, the green spectrum representing the blocking layers likely contains signal from an adjacent region as well. However, the C1s spectra of the blocking layers remain distinct from the red and yellow C1s spectra. The end of the green region is determined by the drop in N1s signal, and thus the yellow hydrogen-bonded region begins. Finally, the black adhesion layer starts when the N1s signal increases at the base of the film because of the presence of nitrogen-containing PDAC. These data reveal that each of the various regions of the multilayer heterostructure illustrated in Fig. 1*B* can be identified in XPS depth-profile spectra.

The N1s spectra from depth-profiling samples with blocking layers were analyzed to determine the atomic percentage of nitrogen with depth, as seen in Fig. 4*B* (N1s spectra from all samples with blocking layers are seen in Fig. S6). From Fig. 4*B*, it is clear that all three electrostatic blocking layers tested $(PAH3/SPS3)_z$ ($z = 0.5, 3.5, 9.5$) with approximate thicknesses of <1 nm, 4 nm, and

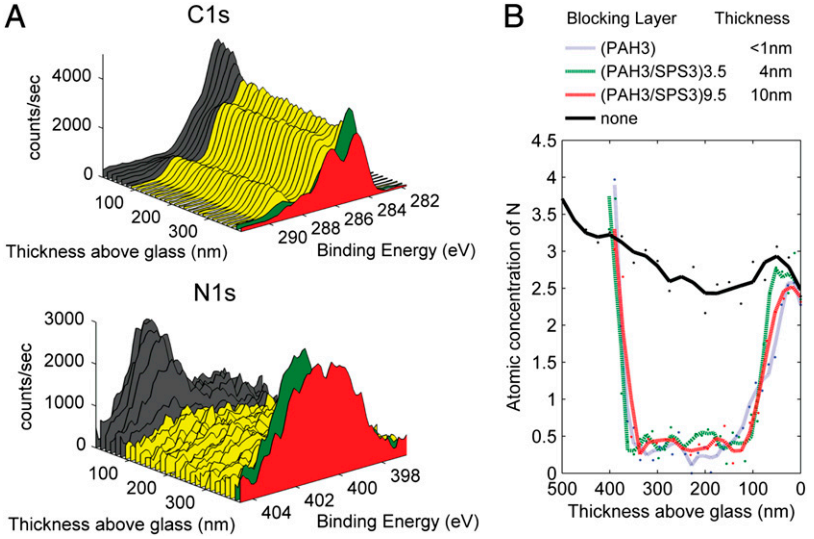

Fig. 4. Effect of a blocking layer on interlayer diffusion of chitosan. (*A*) C1s and N1s regions from depth-profiling XPS of a hydrogen-bonded sample with a $(PAH3/SPS3)_{3.5}$ blocking layer topped with $(HA3/CHI3)_{3.5}$. The color scheme is the same as that of Fig. 1*B*. Red spectra represent (HA3/CHI3), green spectra represent the (PAH3/SPS3) electrostatic blocking layer, yellow spectra represent the (PAA3/PEO3) hydrogen-bonded region, and black spectra represent the (PDAC4/SPS4) adhesion layer. (*B*) Quantification of the nitrogen signal for different blocking-layer systems tested. Data points are individual dots, and the line is the result of a Savitzky–Golay five-point smoothing algorithm. All films had $(HA3/CHI3)_{3.5}$ deposited on top of the blocking layer.

10 nm, respectively, effectively stop the diffusion of chitosan into the hydrogen-bonded region, as seen by the absence of any detectable nitrogen signal in the bulk of the film. Remarkably, even though the films spent over 30 min in chitosan solution during the HA/chitosan film fabrication, even a single adsorbed layer of PAH was sufficient to block its diffusion into the hydrogen-bonded region. At pH 3, PAH is a fully charged polycation (pK_a ~8) (53), so it has a strong electrostatic interaction with the ionizable polyanion PAA found at the top of the hydrogen-bonded region (54). Because of the strong electrostatic interaction, the PAH blocking layer is kinetically trapped at the top of the film (28) and effectively stops the diffusion of chitosan into the hydrogen-bonded region under the conditions used in this study. Recent literature (7, 24, 40, 43, 44) shows that different blocking layers work well for different polymer systems and annealing conditions. In some cases, covalently cross-linked blocking layers are needed (7, 43), but in other cases, electrostatic blocking layers may stop interlayer diffusion as well (24, 44). In the conditions tested in this work, a single electrostatic blocking layer is all that was needed to block the interlayer diffusion of chitosan.

In the absence of a blocking layer, chitosan from the (HA3/CHI3) multilayer film diffuses into the entire hydrogen-bonded film during fabrication, producing a high nitrogen signal throughout, as seen in Fig. 4*B*. Although the film has fewer total layers deposited than the multilayer films with blocking layers, the interlayer diffusion of chitosan allows for a large increase in the final film thickness, as shown by the leftmost data point in Fig. 4*B*. This large increase in thickness is characteristic of exponential growth, which is caused by the diffusion of polymers and polymer pairs in and out of the film during deposition (20). As a result, we expect chitosan, not only from the first bilayer deposition but also from the subsequent depositions, to be present throughout the film. Similar chitosan diffusion into the hydrogen-bonded region also is observed when the order of polymer deposition is switched from HA first (HA3/CHI3) to chitosan first (CHI3/HA3), as revealed in Fig. S7. As a result of macromolecules such as chitosan diffusing throughout a film, hydrogen-bonded films might be used as scaffolds for easy loading of drugs or other macromolecules of interest (3, 55).

An interesting question concerning the use of depth-profiling XPS with C_{60}^+ sputtering is: What level of vertical resolution is possible, and is it sufficient to probe PEM heterostructure interfaces? The interface used to analyze this resolution was the sharp boundary between the (PAH3/SPS3) blocking layers and the hydrogen-bonded region seen in Fig. 4*B*. The precipitous drop of nitrogen signal from the blocking layer to the hydrogen-bonded region occurs between two data points or ~15 nm. Reducing the sputtered thickness between successive XPS spectra would allow the interface resolution to increase to ~10 nm because this commonly is the depth of analysis during an XPS cycle. However, near this limit of resolution, extended sputtering time may cause radiation-induced diffusion and surface roughening, which must be considered during experimental design (48).

pH Sensitivity of the Hydrogen-Bonded Region. The purpose of a blocking layer is to maintain the distinct properties of each region of a multilayer film. In our model system, the as-assembled (PAA3/PEO3) hydrogen-bonded region dissolves above pH 3.6 (47). If the film is altered by sufficient chitosan interlayer diffusion, the multilayer becomes insoluble at neutral pH. Therefore, to test whether the desired properties of the hydrogen-bonded region can be maintained through the use of blocking layers, all films characterized previously were exposed to a buffered salt solution of PBS, pH 7.4, for 30 min. After 30 min, the residual dry film thickness was compared with the initial dry film thickness to determine whether the hydrogen-bonded film dissolved. As seen in Table 2, all multilayer films with a blocking layer dissolved in PBS. Therefore, even a single layer of PAH can effectively block chitosan diffusion and maintain the pH-sensitive solubility of the hydrogen-bonded region.

In the absence of a blocking layer, the multilayer films no longer dissolved because pH-stable electrostatic cross-links formed between the diffused chitosan and PAA. In some cases, such as CHI1, CHI3, and CHI10, this result was unexpected because chitosan did not diffuse all the way through the film (Fig. 2*E*) before PBS exposure. However, depth profiling of CHI10 after PBS exposure shows that chitosan diffused throughout the film and stabilized it to pH changes (Fig. S8). Therefore, in the absence of a blocking layer, chitosan interlayer diffusion was stopped by drying for analysis but continued after exposure to PBS solutions. Because hydrogen-bonded PEMs require a minute or two to dissolve (56), this brief time allows for further chitosan diffusion, rendering the film insoluble in PBS.

Conclusions

XPS with C_{60}^+ cluster ion sputtering is a powerful technique for analyzing the atomic composition and chemical state of organic nanostructured films. With the correct choice of conditions to minimize sample damage, it can determine directly, to within 15 nm, the location of polymers through the thickness of a film, allowing analysis of interlayer diffusion as well as testing of the efficacy of various blocking layers. Using our model system, we have shown that chitosan is highly diffusive, with an interlayer diffusion coefficient $\sim 1.4*10^{-12}$ cm^2/s in hydrated hydrogen-bonded (PAA3/PEO3) films. Also, the high-resolution capabilities of XPS show the displacement of hydrogen-bonded PEO in favor of electrostatic interactions between chitosan and PAA. Finally, various thicknesses of PAH-containing blocking layers were explored, including a single layer of PAH that can stop the diffusion of chitosan into the hydrogen-bonded region.

We believe the ability to control and measure the interlayer diffusion in PEMs will have applications in a variety of areas. For example, exchanging hydrogen-bonding interactions for electrostatic ones may be important for the loading of biological molecules through postassembly modification of films. Furthermore, the design of films capable of blocking macromolecule diffusion is relevant to structured films, sequential drug release, and production of free-floating PEM films.

Materials and Methods

Materials. PAA (Aldrich; M = 450 kDa), PAH (Aldrich; M = 15 kDa), PEO (Polysciences; M = 20 kDa), PDAC (Aldrich; M = 200–350 kDa in 20% aqueous solution), SPS (Aldrich; M = 70 kDa), HA (from *Streptococcus equi*; Fluka; M ~1,580 kDa), acetic acid (Sigma), and low molecular weight chitosan (deacetylation 0.9; Sigma; M = 50–190 kDa) were used as received. The nomenclature for PEMs follows $(poly1X/poly2X)_z$, where X is the pH of the polymer solutions and z is the number of bilayers deposited (one bilayer = poly1 + poly2). A noninteger value of z indicates the assembly was terminated with poly1.

Multilayer Film Deposition. Polymer solutions were made from Milli-Q 18.2-MΩ water. Solutions of PAA, PDAC, and SPS were 0.01 M, and solutions of PEO, HA, and chitosan were 0.1% (wt/vol). CHI solutions included 0.1 M of acetic acid to aid dissolution. PDAC and SPS solutions for the adhesion layer had 0.1 M NaCl at pH 4.0. All other solution pHs were adjusted to pH 3.0 with 1 M HCl and no added salt. Glass substrates were dipped sequentially in the polymer solutions using an automated Zeiss programmable slide stainer or nanoStrata dipping unit. Substrates were held in polymer solutions for 10 min and then rinsed for a total of 3 min in water with mild agitation. The time in chitosan solution was altered for diffusion studies, but the rinse cycle

Table 2. pH sensitivity of the hydrogen-bonded region

Figure	Top layer	Blocking layer	Dissolve in PBS, pH 7.4?
Fig. 4	$(HA3/CHI3)_{3.5}$	(PAH3)	Yes
	$(HA3/CHI3)_{3.5}$	$(PAH3/SPS3)_{3.5}$	Yes
	$(HA3/CHI3)_{3.5}$	$(PAH3/SPS3)_{9.5}$	Yes
	$(HA3/CHI3)_{3.5}$	None	No
Fig. 2	CHI60	None	No
	CHI10	None	No
	CHI3	None	No
	CHI1	None	No

After exposure to pH 7.4 PBS for 30 min, the remaining thickness was compared with the initial thickness to determine whether the hydrogen-bonded region dissolved.

used the same time profiles. Fabrication details and polymer structures are listed in *SI Materials and Methods* and Fig. S9, respectively. Dry film thickness was measured with a P-16 profiler (KLA-Tencor Corp.).

XPS. Chemical composition of the surface was characterized using a PHI VersaProbe II X-ray photoelectron spectrometer with a scanning monochromated Al source (1,486.6 eV; 50 W; spot size, 200 μm). The takeoff angle between the sample surface and analyzer was 45°, and the X-ray beam collected C1s, N1s, O1s, and Si2p elemental information while rastering over a 200 X 700-μm area. Detailed XPS acquisition parameters are found in Table S2. Depth profiling was accomplished using the instrument's C_{60}^{+} ion source operated at 10 kV, 10 nA, and rastered over a 3 × 3-mm area at an angle of 70° to the surface normal. Sputtering occurred in 1-min intervals while the sample was moved using concentric Zalar rotation at 1 rpm. Atomic composition was determined based on photoelectron peak areas and the relative sensitivity factors provided in PHI's MultiPak processing software. All data were background subtracted, smoothed using a five-point quadratic Savitzky–Golay algorithm, and charge corrected so that the carbon–carbon bond had a binding energy of 285.0 eV. The surface of the glass was defined as the point at which the atomic concentration of silicon reached 5% in the depth-profiling data. The thickness as measured by profilometry was compared with the number of sputter cycles that occurred before reaching the surface of the glass. Data were plotted using Matlab.

pH Sensitivity of Hydrogen-Bonded Region. Films were tested by a 30-min immersion in PBS (pH 7.4) on an orbital shaker at 100 rpm. After drying with N_2, the thickness was measured using profilometry and compared with the initial thickness to determine whether the hydrogen-bonded region dissolved.

ACKNOWLEDGMENTS. We acknowledge support by the Materials Research Science and Engineering Centers (MRSEC) Program of the National Science Foundation (NSF) under Award DMR–0819762, as well as the excellent assistance of Libby Shaw of the MRSEC shared facilities. J.B.G. is supported by a National Defense Science and Engineering Graduate (NDSEG) and NSF fellowship.

1. Cebeci FC, Wu ZZ, Zhai L, Cohen RE, Rubner MF (2006) Nanoporosity-driven superhydrophilicity: A means to create multifunctional antifogging coatings. *Langmuir* 22(6):2856–2862.
2. Hiller J, Mendelsohn JD, Rubner MF (2002) Reversibly erasable nanoporous anti-reflection coatings from polyelectrolyte multilayers. *Nat Mater* 1(1):59–63.
3. Boudou T, Crouzier T, Ren KF, Blin G, Picart C (2010) Multiple functionalities of polyelectrolyte multilayer films: New biomedical applications. *Adv Mater (Deerfield Beach Fla)* 22(4):441–467.
4. Zelikin AN (2010) Drug releasing polymer thin films: New era of surface-mediated drug delivery. *ACS Nano* 4(5):2494–2509.
5. Swiston AJ, et al. (2008) Surface functionalization of living cells with multilayer patches. *Nano Lett* 8(12):4446–4453.
6. Doshi N, et al. (2011) Cell-based drug delivery devices using phagocytosis-resistant backpacks. *Adv Mater (Deerfield Beach Fla)* 23(12):H105–H109.
7. Wood KC, Chuang HF, Batten RD, Lynn DM, Hammond PT (2006) Controlling interlayer diffusion to achieve sustained, multiagent delivery from layer-by-layer thin films. *Proc Natl Acad Sci USA* 103(27):10207–10212.
8. Lutkenhaus JL, Hammond PT (2007) Electrochemically enabled polyelectrolyte multilayer devices: From fuel cells to sensors. *Soft Matter* 3(7):804–816.
9. Lavalle P, et al. (2011) Dynamic aspects of films prepared by a sequential deposition of species: Perspectives for smart and responsive materials. *Adv Mater (Deerfield Beach Fla)* 23(10):1191–1221.
10. Decher G (1997) Fuzzy nanoassemblies: Toward layered polymeric multicomposites. *Science* 277(5330):1232–1237.
11. Zhai L, Nolte AJ, Cohen RE, Rubner MF (2004) Ph-gated porosity transitions of polyelectrolyte multilayers in confined geometries and their application as tunable Bragg reflectors. *Macromolecules* 37(16):6113–6123.
12. Hammond PT (2011) Engineering materials layer-by-layer: Challenges and opportunities in multilayer assembly. *AIChE J* 57(11):2928–2940.
13. Wu Z, Lee D, Rubner MF, Cohen RE (2007) Structural color in porous, superhydrophilic, and self-cleaning SiO2/TiO2 Bragg stacks. *Small* 3(8):1445–1451.
14. Kim JK, et al. (2012) Ultrathin nanoclay films with tunable thickness as barrier layers in organic light emitting devices. *J Mater Chem* 22(16):7718–7723.
15. Kim KH, et al. (2012) Interface control with layer-by-layer assembled ionic polymers for efficient low-temperature dye-sensitized solar cells. *J Mater Chem* 22(22):11179–11184.
16. Cho J, Caruso F (2003) Polymeric multilayer films comprising deconstructible hydrogen-bonded stacks confined between electrostatically assembled layers. *Macromolecules* 36(8):2845–2851.
17. Podsiadlo P, et al. (2009) Diffusional self-organization in exponential layer-by-layer films with micro- and nanoscale periodicity. *Angew Chem Int Ed Engl* 48(38):7073–7077.
18. Yoo PJ, et al. (2008) Controlling surface mobility in interdiffusing polyelectrolyte multilayers. *ACS Nano* 2(3):561–571.
19. Francius G, et al. (2007) Stiffening of soft polyelectrolyte architectures by multilayer capping evidenced by viscoelastic analysis of AFM indentation measurements. *J Phys Chem C* 111(23):8299–8306.
20. Picart C, et al. (2002) Molecular basis for the explanation of the exponential growth of polyelectrolyte multilayers. *Proc Natl Acad Sci USA* 99(20):12531–12535.
21. Lavalle P, et al. (2004) Direct evidence for vertical diffusion and exchange processes of polyanions and polycations in polyelectrolyte multilayer films. *Macromolecules* 37(3):1159–1162.
22. Haynie DT, Cho EH, Waduge P (2011) "In and out diffusion" hypothesis of exponential multilayer film buildup revisited. *Langmuir* 27(9):5700–5704.
23. Porcel C, et al. (2007) Influence of the polyelectrolyte molecular weight on exponentially growing multilayer films in the linear regime. *Langmuir* 23(4):1898–1904.
24. Garza JM, et al. (2004) Multicompartment films made of alternate polyelectrolyte multilayers of exponential and linear growth. *Langmuir* 20(17):7298–7302.
25. Richert L, et al. (2004) Layer by layer buildup of polysaccharide films: Physical chemistry and cellular adhesion aspects. *Langmuir* 20(2):448–458.
26. Lundin M, Blomberg E, Tilton RD (2010) Polymer dynamics in layer-by-layer assemblies of chitosan and heparin. *Langmuir* 26(5):3242–3251.
27. Lee L, Johnston APR, Caruso F (2012) Probing the dynamic nature of DNA multilayer films using Förster resonance energy transfer. *Langmuir* 28(34):12527–12535.
28. Zacharia NS, Modestino M, Hammond PT (2007) Factors influencing the interdiffusion of weak polycations in multilayers. *Macromolecules* 40(26):9523–9528.
29. Soltwedel O, et al. (2010) Interdiffusion in polyelectrolyte multi layers. *Macromolecules* 43(17):7288–7293.
30. Xu L, Ankner JF, Sukhishvili SA (2011) Steric effects in ionic pairing and polyelectrolyte interdiffusion within multilayered films: A neutron reflectometry study. *Macromolecules* 44(16):6518–6524.
31. Jomaa HW, Schlenoff JB (2005) Salt-induced polyelectrolyte interdiffusion in multilayered films: A neutron reflectivity study. *Macromolecules* 38(20):8473–8480.
32. Arys X, Laschewsky A, Jonas AM (2001) Ordered polyelectrolyte "Multilayers". 1. Mechanisms of growth and structure formation: A comparison with classical fuzzy "Multilayers." *Macromolecules* 34(10):3318–3330.
33. Nobuta T, Ogawa T (2009) Depth profile XPS analysis of polymeric materials by c-60 (+) ion sputtering. *J Mater Sci* 44(7):1800–1812.
34. Szakal C, Sun S, Wucher A, Winograd N (2004) C-60 molecular depth profiling of a model polymer. *Appl Surf Sci* 231:183–185.
35. Hollander A, Haupt M, Oehr C (2007) On depth profiling of polymers by argon ion sputtering. *Plasma Process Polym* 4(9):773–776.
36. Chen YY, et al. (2008) X-ray photoelectron spectrometry depth profiling of organic thin films using C60 sputtering. *Anal Chem* 80(2):501–505.
37. Yu BY, et al. (2008) Depth profiling of organic films with X-ray photoelectron spectroscopy using C60+ and Ar+ co-sputtering. *Anal Chem* 80(9):3412–3415.
38. Postawa Z, et al. (2004) Microscopic insights into the sputtering of ag{111} induced by C60 and Ga bombardment. *J Phys Chem B* 108(23):7831–7838.
39. Mahoney CM (2010) Cluster secondary ion mass spectrometry of polymers and related materials. *Mass Spectrom Rev* 29(2):247–293.
40. Zacharia NS, DeLongchamp DM, Modestino M, Hammond PT (2007) Controlling diffusion and exchange in layer-by-layer assemblies. *Macromolecules* 40(5):1598–1603.
41. Mertz D, et al. (2009) Mechanotransductive surfaces for reversible biocatalysis activation. *Nat Mater* 8(9):731–735.
42. Hong J, et al. (2012) Graphene multilayers as gates for multi-week sequential release of proteins from surfaces. *ACS Nano* 6(1):81–88.
43. Peralta S, Habib-Jiwan JL, Jonas AM (2009) Ordered polyelectrolyte multilayers: Unidirectional FRET cascade in nanocompartmentalized polyelectrolyte multilayers. *ChemPhysChem* 10(1):137–143.
44. Salomäki M, Kankare J (2009) Influence of synthetic polyelectrolytes on the growth and properties of hyaluronan-chitosan multilayers. *Biomacromolecules* 10(2):294–301.
45. Mertz D, et al. (2007) Mechanically responding nanovalves based on polyelectrolyte multilayers. *Nano Lett* 7(3):657–662.
46. Okamura Y, Kabata K, Kinoshita M, Saitoh D, Takeoka S (2009) Free-standing biodegradable poly(lactic acid) nanosheet for sealing operations in surgery. *Adv Mater (Deerfield Beach Fla)* 21(43):4388–4392.
47. DeLongchamp DM, Hammond PT (2004) Highly ion conductive poly(ethylene oxide)-based solid polymer electrolytes from hydrogen bonding layer-by-layer assembly. *Langmuir* 20(13):5403–5411.
48. Shard AG, Green FM, Gilmore IS (2008) C(60) ion sputtering of layered organic materials. *Appl Surf Sci* 255(4):962–965.
49. Beamson G, Briggs D (1992) *High Resolution XPS of Organic Polymers: The Scienta ESCA300 Database* (Wiley, Chichester).
50. Crank J (1975) *The Mathematics of Diffusion* (Clarendon, Oxford), 2nd Ed.
51. Kharlampieva E, Kozlovskaya V, Ankner JF, Sukhishvili SA (2008) Hydrogen-bonded polymer multilayers probed by neutron reflectivity. *Langmuir* 24(20):11346–11349.
52. Hübsch E, et al. (2005) Multivalent ion/polyelectrolyte exchange processes in exponentially growing multilayers. *Langmuir* 21(8):3664–3669.
53. Choi J, Rubner MF (2005) Influence of the degree of ionization on weak polyelectrolyte multilayer assembly. *Macromolecules* 38(1):116–124.
54. Shiratori SS, Rubner MF (2000) Ph-dependent thickness behavior of sequentially adsorbed layers of weak polyelectrolytes. *Macromolecules* 33(11):4213–4219.
55. Yuan WY, Lu ZS, Wang HL, Li CM (2012) Stimuli-free reversible and controllable loading and release of proteins under physiological conditions by exponentially growing nanoporous multilayered structure. *Adv Funct Mater* 22(9):1932–1939.
56. Lutkenhaus JL, Hrabak KD, McEnnis K, Hammond PT (2005) Elastomeric flexible free-standing hydrogen-bonded nanoscale assemblies. *J Am Chem Soc* 127(49):17228–17234.